INDONESIAN SCHOLAR SOCIETY

Indones. J. Chem. Stud.
2024, 3(1), 8–15
Available online at journal.solusiriset.com
e-ISSN: 2830-7658; p-ISSN: 2830-778X

Indonesian Journal of Chemical Studies

Magnetically Chitosan-Silica-Based Biosorbent as Efficient Removal of Au(III) in Artificial Wastewater

Adya Rizky Pradipta[1]*, Regita Andriani Wiana Putri[2], Inna Yusnila Khairani[3], Lutfi Aditya Hasnowo[4]

[1]*Department of Food Nanotechnology, AKA Bogor Polytechnic, Jl. Pangeran Sogiri No. 283, Bogor 16154, Indonesia*

[2]*Department of Chemistry, Republic of Indonesia Defense University, Kawasan IPSC Sentul, Bogor 16810, Indonesia*

[3]*University of Wuppertal, Gaußstraße 20, Wuppertal, North Rhine-Westphalia State 42119, Germany*

[4]*School of Nuclear Science and Engineering, Tomsk Polytechnic University, Tomsk, Tomsk Oblast 634050, Russia*

Received: 23 Jan 2024; Revised: 24 Feb 2024; Accepted: 25 Feb 2024;
Published online: 27 Mar 2024; Published regularly: 30 Jun 2024

Abstract— The synthesis of chitosan-modified silica-coated iron oxide magnetic material (Fe_3O_4/SiO_2/Chitosan) via the sol-gel process addresses the need for enhanced stability and functionality in various applications. Coating iron oxide magnetic material with chitosan-modified silica is a common strategy to improve biocompatibility and performance. This study investigates the synthesis of Fe_3O_4/SiO_2/Chitosan using sodium silicate as the silica precursor. The synthesis involved sonication of Fe_3O_4 and sodium silicate for 5 min, followed by adding chitosan in 4% acetic acid with continuous stirring. The mass ratio of Fe_3O_4:SiO_2 was fixed at 0.5:0.73, with varying chitosan masses (0.025, 0.050, and 0.075 g). Characterization techniques used included Fourier-Transform Infrared Spectroscopy (FTIR), X-ray powder Diffraction (XRD), and Thermogravimetric analysis (TGA). The product with the highest mass yield was further analyzed. The variation in the amount of chitosan in the conducted research aimed to determine the optimum chitosan mass that could still bind to the silica framework. Magnetite was confirmed as the primary composition, with the addition of chitosan and silica functional groups observed through vibration absorption characteristics. Thermogravimetric analysis showed differences in decomposition patterns between samples. The optimal chitosan content for characterization was determined at 0.050 g. Future applications might include enhanced adsorption processes owing to the optimized structure and composition of Fe_3O_4/SiO_2/Chitosan nanoparticles.

Keywords— *Adsorption; Gold(III) adsorption; Iron oxide nanoparticles; Silica-chitosan coating; Sol-gel synthesis*

1. INTRODUCTION

Gold is a metal that has been extensively studied due to its inert, soft, and malleable properties, making it suitable for various applications, such as electronic components, coatings, photography, metal alloys, catalysts, and medical purposes. The gold processing industry generates gold waste as a by product, which often enters water systems through rivers commonly used by the surrounding population. Gold contamination in water systems poses challenges for gold recovery processes and leads to environmental pollution [1].

Several techniques and methods for heavy metal (including gold) waste treatment have been explored, including chemical precipitation in basic conditions [2], coagulation-flocculation [3], membrane filtration [4], ion exchange [5], and adsorption [6]. Chemical precipitation involves the formation of insoluble metal hydroxide complexes ($M(OH)_n$). Basic conditions for precipitation require high concentrations of base (corrosive) and result in sludge formation, leading to the creation of new deposits [7]. Coagulation and flocculation techniques aim to stimulate particle collisions to form floccules that can be easily precipitated. However, these methods also produce a mixture of sludge, requiring additional separation techniques [8].

Ion exchange exhibits high effectiveness but generates secondary pollutants and necessitates further separation. Membrane filtration and ion exchange, while selective, are less effective and involve

***Corresponding author**.
Email address: adya.rizky@solusiriset.com
DOI: 10.55749/ijcs.v3i1.40

relatively high operational costs [9]. Adsorption, on the other hand, is a relatively simple and cost-effective technique commonly used for metal separation in water environments.

Silica-based materials have been extensively researched and employed as adsorbents due to their flexible structure, heat resistance, mechanical stability, and large surface area [10]. The silica surface can be modified with other functional groups to enhance its adsorption effectiveness and selectivity for metal ions. The addition of amino groups, known for their strong interactions with metals, is one such modification.

Commonly, synthetic reagents like (N-(2-aminoethyl)-3-aminopropyl)[11], (3-aminopropyl) triethoxysilane [12], and N-(3-trimethoxysilylpropyl)diethylenetriamine [13] are used to modify silica surfaces. However, the use of synthetic materials is considered less economical due to the expensive precursors. An alternative source of amino groups is chitosan, a natural polymer derived from crustacean shells, known for its biocompatibility and environmental friendliness.

Despite the advantages of adsorption, the separation of adsorbent and adsorbate remains a challenge. Conventional separation methods, like filtration, are considered less effective due to prolonged processing times. An alternative for adsorbent separation is magnetic separation, utilizing magnetic materials in the adsorbent system. This method is more effective, environmentally friendly, and does not incur high operational costs [14].

Iron oxide, particularly magnetite, is a widely recognized magnetic material. The magnetic force exhibited by magnetite renders it a suitable candidate for this purpose. However, magnetic materials are susceptible to leaching and rusting in corrosive environments. Coating the surface of the magnetic materials with a stable substance under acidic conditions can effectively mitigate these issues [15].

Silica precursor tetraethyl orthosilicate (TEOS) is commonly used, but its utilization results in the by product alcohol [16]. An alternative silica precursor, sodium silicate (Na_2SiO_3), derived from natural resources like rice husk ash, can minimize the formation of alcohol byproducts. The sol-gel method is a commonly used technique for silica modification due to its simplicity, speed, and low-temperature synthesis, making it environmentally friendly.

Previous studies have revealed that the optimum pH in the adsorption process of heavy metals using chitosan-silica hybrids is pH 3 [17]. The explanation regarding the optimum conditions for metal adsorption by chitosan is that at pH 3, the protonation of amino groups on the adsorbent surface forms $-NH_3^+$ groups that are optimal for electrostatic interaction with $AuCl_4^-$ species. The interaction between the amino species and gold(III) occurs through two predicted interactions, namely between the protonated amino groups and $AuCl_4^-$ species and between deprotonated amino groups and gold(III) [18].

Research on the synthesis of magnetite coated with silica and chitosan involves investigating the influence of adding chitosan mass on the resulting product mass. Material characterization involves the identification of functional groups, crystallinity, material composition, morphology, and thermal analysis. Subsequent studies include examining the pH influence on gold(III) adsorption.

2. EXPERIMENTAL SECTION

2.1. Materials

The materials employed in this investigation consisted of ferric chloride hexahydrate ($FeCl_3 \cdot 6H_2O$), ferrous sulfate heptahydrate ($FeSO_4 \cdot 7H_2O$) (Merck), chitosan sourced from CV Ocean Fresh Bandung (in flake form, derived from crab shells, possessing a degree of deacetylation >80%), 96% acetic acid (Merck), 37% hydrochloric acid (Merck), 65% nitric acid (Merck), sodium silicate (Merck), sodium citrate (Merck), sodium hydroxide (Merck), 24k gold bullion from PT Antam, distilled water, and Aquabidest.

2.2. Instrumentations

The equipment employed in the experiment included glassware, external magnets, ultrasonic bath (Krisbow), universal pH indicator (Merck), marble mortar, 200-mesh sieve, plastic containers, oven (Isotemp Oven Model 655F), grinder (Memmert), and analytical balance (Mettler Toledo). The instrumentation used in characterization and analysis included FTIR Spectrometer (IR PRESTIGE-21 SHIMADZU), X-Ray Diffractometer/XRD (Shimadzu Japan Type XRD Lab.-X XRD-6000), Scanning Thermal Analysis/TGA (NETZSCH STA 449 F1), pH meter (SI Analytics Lab 860), and Atomic Absorption Spectrometer (Perkin Elmer 3110).

2.3. Synthesis of Magnetic Iron Oxide Nanoparticles

A total of 3.01 g $FeCl_3 \cdot 6H_2O$ and 2.04 g $FeSO_4 \cdot 7H_2O$ were individually dissolved in 30 mL of deionized water while being purged with N_2 gas. The solution was sonicated, and NaOH 25% was added dropwise until reaching pH 10. Subsequently, 1 g of sodium citrate was added to the solution, and sonication was continued for 30 h. The solution was washed with deionized water until reaching pH 7 and then dried at 80 °C for 8 h.

2.4. Synthesis of Fe_3O_4/SiO_2 and Fe_3O_4/SiO_2/Chitosan

Different amounts of chitosan (0.025; 0.050; and 0.075 g) were dissolved in 13 mL of 4% acetic acid with magnetic stirring for 45-60 min, followed by overnight standing. 0.5 g of $FeCl_3$ was placed in a plastic container, washed with 1 mL of 1 M HCl, and magnetically separated. A volume of 2 mL of p.a. sodium silicate was added to the magnetite, and 4 mL of distilled water was

added before sonicating for 5 min. For each variation, the chitosan solution was slowly introduced into the plastic container containing $FeCl_3$ and silica with simultaneous mechanical stirring.

The synthesis of Fe_3O_4/SiO_2 was carried out using the same procedure (without chitosan), involving the addition of 4% acetic acid to sonicated Fe_3O_4/SiO_2. For Fe_3O_4/SiO_2 and Fe_3O_4/SiO_2/Chitosan, aging was conducted overnight, followed by drying at 80 °C for 7 h. The solid was then washed and redried at 80 °C, then gently ground without sieving. The resulting product was weighed, and FTIR characterization was performed. The product with the highest mass yield was further characterized using XRD and TGA as Fe_3O_4/SiO_2/Chitosan

2.5. Study of pH Influence on Gold(III) Adsorption

Aqua regia solution was prepared by mixing three parts of concentrated nitric acid and one part of concentrated hydrochloric acid. The preparation of gold(III) chloride solution was done by dissolving 24k gold bullion in aqua regia solution. Gold(III) adsorption was carried out by adding 10 mg of the adsorbent into 10 mL of $AuCl_4^-$ 100 ppm solution at different pH levels (1, 2, 3, 4, 5, and 6). Stirring was performed for 2 h. The separation of the adsorbent from the adsorbate was carried out magnetically, and the remaining solution was analyzed using AAS.

3. RESULT AND DISCUSSION

3.1. Synthesis of Fe_3O_4/SiO_2/Chitosan

The coating of magnetite with chitosan-modified silica begins with magnetite synthesis. The synthesis of magnetite (Fe_3O_4) in this study was conducted using the coprecipitation method. A mixture of Fe^{3+} and Fe^{2+} salts with a molar ratio of Fe^{3+}:Fe^{2+}= 2:1 was precipitated by the slow addition of NaOH solution (dropwise). NaOH base was utilized as the precipitating agent in the magnetite synthesis process. The activation of Fe_3O_4 was followed by the addition of sodium silicate (Na_2SiO_3) and water, followed by sonication. Ultrasonic waves can reduce the size of solids through solid disruption, thereby increasing the solid's surface contact with the solvent. This method facilitates the disintegration of Fe_3O_4 particles into smaller particles and prevents Fe_3O_4 aggregation, thereby allowing dispersion within the silica system. At this stage, partial condensation may occur due to the possible presence of hydrochloric acid solution along with Fe_3O_4 solids. Under acidic conditions, silica condensation may occur, forming siloxane bridges on the Fe_3O_4 surface.

The Fe_3O_4/SiO_2 mixture was sonicated gently, accompanied by mechanical stirring. The acidic conditions formed by acetic acid as the chitosan solvent support the sol-gel process in the siloxane bridge formation. The acidic medium can catalyze the sol-gel process through acid-catalyzed hydrolysis. Condensation of silanol groups with -OH groups in chitosan occurs, followed by water loss (hydrolysis). Mechanical stirring aims to increase collision contact between reagent particles and evenly distribute the acidic environment in the system. The magnetic Fe_3O_4, silica, and chitosan materials were mixed simultaneously in a single container to prevent reagent loss due to displacement. The resulting gel pH was 6. Aging is conducted overnight to stabilize the formed gel and strengthen the bonds of each material. The resulting material appeared black and formed an inseparable colloid between each material. Drying in a moderate-temperature oven aims to remove absorbed water molecules from the composite, while washing is performed to eliminate ions, including acetate and sodium ions, that may be attached to the synthesized material. High-temperature drying is avoided to prevent damage to chitosan, which is an organic polymer. The resulting product after drying is referred to as xerogel. The variation in the amount of chitosan in the conducted research aims to determine the optimum chitosan mass that could still bind to the silica framework. The products from each chitosan variation were weighed and characterized using FTIR. The mass of the synthesized products is presented in **Table 1**.

Table 1. Comparison of product mass with variations in the amount of chitosan

Amount of chitosan (g)	Mass of Fe_3O_4/SiO_2/Chitosan (g)
0	1.4422
0.025	1.5622
0.050	1.7482
0.075	1.4415

Based on **Table 1**, there was an increase in the product mass up to the addition of 0.050 g of chitosan, but then it decreased with the addition of 0.075 g of chitosan. This indicates the amount of chitosan that can be accommodated within the optimum composite framework at the addition of 0.050 g of chitosan. The addition of 0.075 g of chitosan may lead to a tendency for chitosan to form hybrids with silica, which are detached from iron oxide bonds due to an excess of chitosan, where the chitosan-silica hybrid is detached from the magnetic system due to stronger interaction between chitosan and silica compared to chitosan-silica hybrids with Fe_3O_4. Chitosan-silica hybrids not bound to Fe_3O_4 can be lost through washing and magnetic separation treatments. The highest mass product, 0.050 g chitosan variation, was further characterized with XRD and TGA as Fe_3O_4/SiO_2/Chitosan.

3.2. X-Ray Diffraction Patterns of Fe_3O_4 and Fe_3O_4/SiO_2/Chitosan

Fe_3O_4 and iron oxide magnetic materials coated with chitosan-modified silica (Fe_3O_4/SiO_2/Chitosan), which had been dried, were characterized using an X-ray diffractometer to observe the crystallinity and

composition of minerals present. **Fig. 1** provides information regarding the X-ray diffraction patterns of Fe_3O_4 and Fe_3O_4/SiO_2/Chitosan.

Mineral identification in Fe_3O_4 was conducted by matching the X-ray diffraction pattern of Fe_3O_4 (**Fig. 1a.**) with the synthetic Fe_3O_4 reference from ICDD 00-019-0629. The characteristic planes of Fe_3O_4 were detected at planes hkl [111], [220], [311], [400], [511], and [440]. These results are in accordance with those obtained by Pradipta (2022) [14]. At 2θ = 29.52, the diffraction intensity was sufficiently high, possibly due to the presence of Sodium contamination (ICDD 00-001-0850) originating from the synthesis of Fe_3O_4. A decrease in intensity indicates a reduction in crystallinity or structural regularity of the material. Broad peaks observed at 2θ = 15-25° indicate an amorphous phase of silica covering the [111] plane of the magnetite crystals. The characteristic chitosan diffraction peaks at 2θ = 8.6; 11.7; 15.1; and 20.6° [19] overlapped with the broad peaks characteristic of amorphous silica.

Upon closer inspection of the characteristic peaks in Fe_3O_4 and Fe_3O_4/SiO_2/Chitosan, the coating led to a significant reduction in peak intensity at the hkl [220] plane compared to the reduction in intensity at the hkl [311] plane. This suggests that the coating is more inclined to cover the [220] plane than the [311] plane in magnetite. The decrease in intensity at the [220] plane, specifically at 2θ = 29.52°, could also be attributed to the removal of minerals.

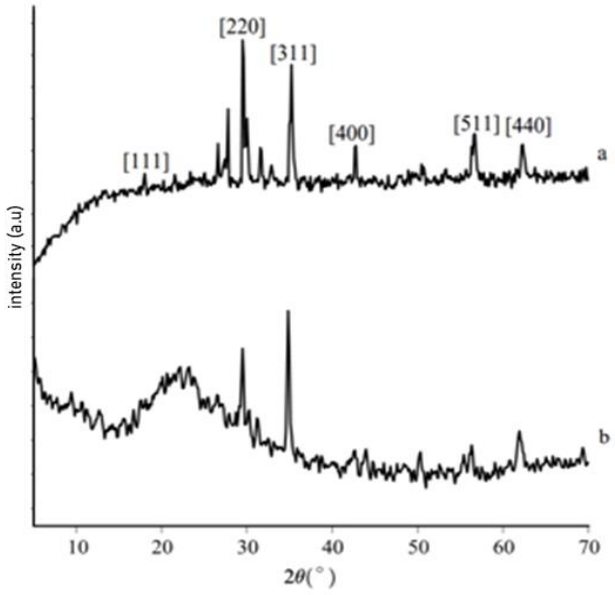

Fig. 1 X-ray diffraction patterns of a) Fe_3O_4 and b) Fe_3O_4/SiO_2/Chitosan

3.3. Infrared Spectroscopy Characterization of Silica and Chitosan-Coated Iron Oxide Magnetic Material

To ensure the successful coating of silica and chitosan on the surface of the iron oxide magnetic material, the identification of functional groups was carried out through infrared spectroscopy characterization. The characteristic vibrations of functional groups were examined when subjected to infrared radiation.

The infrared spectrum of Fe_3O_4 (**Fig. 2a.**) reveals characteristic vibrations at the wavenumber of 570.9 cm^{-1}, corresponding to the Fe-O group vibration of magnetite mineral. Broad absorptions at 3448.7 cm^{-1} and 1635.6 cm^{-1} indicate the contribution of absorbed water molecules, signifying –OH group vibrations. Additional absorptions at 1064.7 cm^{-1} (vibration of Si-O-Si) and 478.4 cm^{-1} (bending vibration of Si-O-Si) confirm the presence of silica in the composite.

Chitosan's characteristic absorptions included a broad peak in the range of 3400-3600 cm^{-1}, indicating the overlap of –OH and –NH stretching vibrations. Vibrations of methylene groups were observed at 2924 cm^{-1}. Specific peaks include the carbonyl group stretching vibration at 1635 cm^{-1}, overlapping with –OH vibrations, and the deformation vibration of $-NH_2$ at 1543 cm^{-1}.

The infrared spectrum of silica-coated iron oxide magnetic material (Fe_3O_4/SiO_2) (**Fig. 2c**) shows characteristic intensities in the 1000-1100 and 470 cm^{-1} regions, representing silica vibrations. Absorptions at 3300-3500 cm^{-1} and 1600-1700 cm^{-1} indicate –OH vibrations from the absorbed water. A peak at 794.7 cm^{-1} suggests the presence of Si-O-Fe bonding.

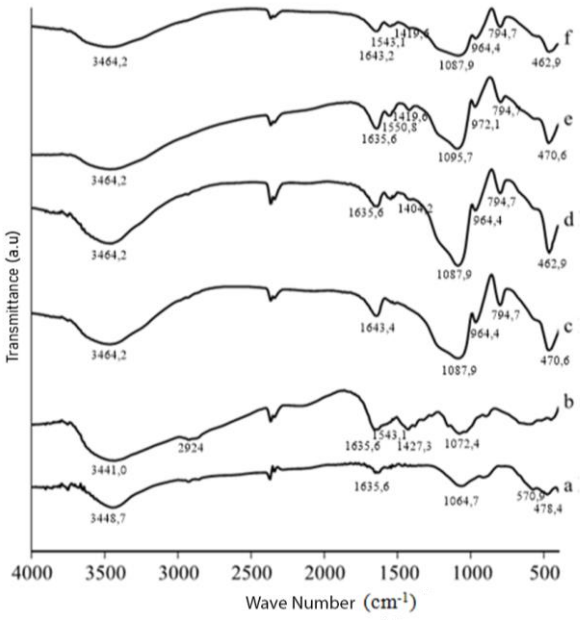

Fig. 2 Infrared spectra of a) Fe_3O_4; b) chitosan; c) Fe_3O_4/SiO_2; d) Fe_3O_4/SiO_2/Chitosan0.025g; e)Fe_3O_4/SiO_2/Chitosan0.050g; and f) Fe_3O_4/SiO_2/Chitosan0.075g

The successful coating of silica modified with chitosan on the surface of iron oxide magnetic material combines the absorption characteristic of all three materials in the infrared spectrum. In the three variations of chitosan addition (**Fig. 2d-2f**), the characteristic absorptions of $-NH_2$ deformation at 1550

cm^{-1}, C=O stretching at 1656 cm^{-1}, and C-N axial deformation at 1419 cm^{-1} were observed. Overlapping vibrations, such as C-O stretching with Si-O vibrations at 1070 cm^{-1}, were possible.

The infrared spectra of the three variations of chitosan addition showed no significant shifts but changes in intensity were evident. A decrease in intensity in the 3300-3500 cm^{-1} region suggests a reduction in absorbed water, indicating that the more chitosan added, the smaller the water absorption capacity of the composite. The reduction in silica characteristic vibrations at 1000-1100 cm^{-1} (Si-O-Si bending) and 470 cm^{-1} (Si-O-Si stretching) also supports the hypothesis of decreased silica content in the composite.

The reduction in silica intensity can be explained by an increase in chitosan mass, leading to more chitosan binding to silica and covering the surface of Fe_3O_4. This explanation is supported by the mass data, where the product mass increases up to the 0.050 g chitosan addition, likely due to increased polymer (chitosan) mass and absorbed water. The decrease in product mass at the 0.075 g chitosan addition may be attributed to the formation of chitosan-silica hybrids that detach from the iron oxide magnetic material.

The interactions of the three materials are predicted through the identified infrared absorptions, matched with relevant literature. The presence of Fe-O-Si bonding in the Fe_3O_4/SiO_2/Chitosan composite was confirmed by the uniform absorption at 794 cm^{-1}. Contrary to the proposed Si-O-C covalent interaction by Sugie (2021) [20], no characteristic vibration was observed in the infrared spectrum. Some studies propose a weak interaction [21], capturing chitosan within the silica network. In contrast, other research explains the formation of hybrid materials through interactions between hydroxyl groups on inorganic particle surfaces and active groups on polymers [22].

The prediction of interactions among materials is illustrated in **Fig. 3**. Condensation and hydrolysis lead to the formation of siloxane bridges and silanol groups on the silica surface. Despite the absence of evidence supporting covalent bonds between silica and chitosan in the infrared spectra, the predicted interaction is suggested to be relatively weak hydrogen bonding, involving the entrapment of chitosan within the silica matrix. The formation of hydrogen bonds allows the binding of amine groups (-NH_2), acting as active sites in the metal adsorption process. This may potentially reduce metal adsorption due to the decreased active sites on the composite.

Oxygen species in **Fig. 3**, situated on the surface of the iron oxide magnetic material, could be bound to more than one silica group in random directions (not perfectly illustrated in the scheme). However, the weak interaction between chitosan and silica results in a limited amount of chitosan trapped in the composite. The feeble interaction between chitosan and silica may lead to chitosan loss during washing and magnetic separation processes.

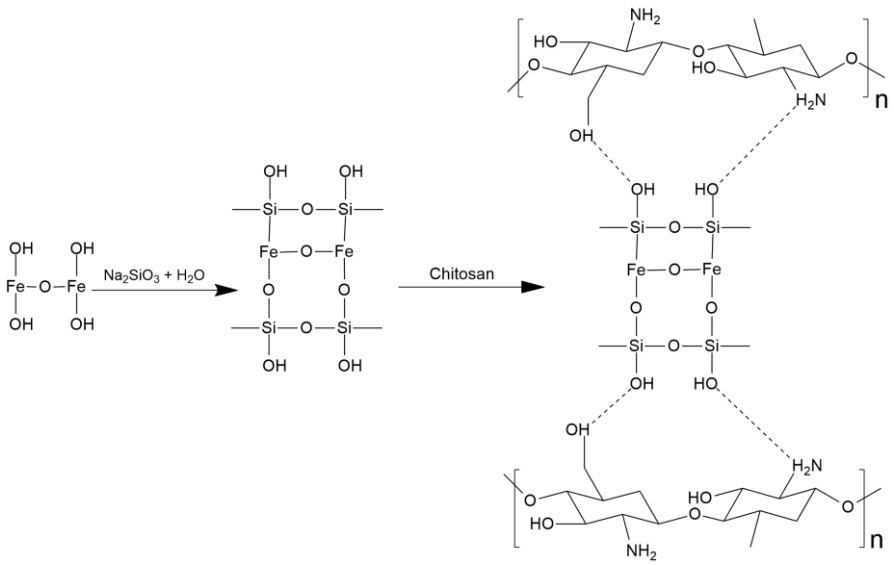

Fig. 3 Prediction of interactions among Fe_3O_4, SiO_2, and chitosan

3.4. Thermal Gravimetric Analysis (TGA)

Thermal gravimetric analysis was conducted on Fe_3O_4/SiO_2 and Fe_3O_4/SiO_2/Chitosan to quantitatively determine the chitosan organic content in the composite. This analysis is based on the observed mass degradation with increasing temperature. The samples were heated from room temperature to a specific temperature while changes in mass were monitored. In the Fe_3O_4/SiO_2 composite, iron oxide and silica are relatively inorganic materials with high thermal stability. The mass reduction is primarily caused by the loss of water molecules from the composite and possibly due to the further condensation of silanol groups in the composite. The results of the gravimetric analysis of the Fe_3O_4/SiO_2 and Fe_3O_4/SiO_2/Chitosan samples are presented in **Fig. 4**.

Based on the TG curves, for both Fe_3O_4/SiO_2 and Fe_3O_4/SiO_2/Chitosan, rapid mass degradation occurred at room temperature up to 140 °C, indicating the loss of water (dehydration) on the composite surface due to the presence of easily water-absorbing silanol groups. The TG curve of the Fe_3O_4/SiO_2 material showed slower mass degradation from 140 to 800 °C. This is possible because the water loss occurs from the deeper part of the composite.

The presence of water in the composite may persist despite the final synthesis stage's drying, as the temperature of 80 °C may not be sufficient to evaporate all the water in the composite. Meanwhile, in Fe_3O_4/SiO_2/Chitosan, a significant difference was observed in the mass degradation curve shape, predicted to be due to the presence of chitosan as an organic content in the composite. The presence of chitosan in the composite requires sufficient heat to degrade the organic material, resulting in slower mass degradation compared to Fe_3O_4/SiO_2, observed from 140 °C to 340 °C. Chitosan's mass degradation is related to the first stage of water release from chitosan at temperatures of 130-200 °C and the second stage, which is chitosan decomposition at temperatures of 200-380 °C, consistent with the thermal decomposition on the TG curve of pure chitosan observed by Gierszewska et al. (2019) [23].

Through gravimetric analysis, the mass changes of Fe_3O_4/SiO_2 and Fe_3O_4/SiO_2/Chitosan were determined to be 3.77% and 5.40%, respectively. The difference in mass changes of 1.63% is predicted to be the contribution of chitosan organic material contained in the composite. Based on this data, it is revealed that the contribution of the chitosan amount trapped in the composite is only 1.63% of the total mass of the Fe_3O_4/SiO_2/Chitosan composite. The limited amount of chitosan trapped in the iron oxide magnetic material framework, binding with sand, is due to the weak interaction between chitosan and silica, in accordance with the predicted interaction from the infrared spectrum data.

The amount of chitosan degraded by 1.63% did not align with the theoretical mass calculation of the composite, where the theoretical % mass of chitosan was 3.91% of the total composite mass. The significant difference between theoretical mass and mass analyzed by thermal gravimetric analysis may be attributed to the loss of a portion of chitosan during washing and magnetic separation due to the weak chitosan-silica bond. Therefore, based on this data, the amount of chitosan trapped in the composite system was only 1.63% of the total composite mass.

3.5. Influence of pH on Gold(III) Adsorption in $AuCl_4^-$ Solution

The study on gold(III) adsorption was conducted using an $HAuCl_4$ solution obtained by dissolving gold in aqua regia, where gold species have an oxidation state of +3. Determining the optimum pH in gold(III) adsorption is crucial to understanding the optimal conditions, which can later be used as a constant variable for other adsorption study parameters (adsorption time variations, concentration variations, adsorption kinetics). The optimum pH was determined using Fe_3O_4/SiO_2/Chitosan adsorbent with pH variations ranging from 1 to 6. The pH variations were assumed based on the general acidity of the water systems (e.g., rivers) with a pH of 6 or slightly acidic.

The separation method employed in the adsorption process is magnetic separation, offering an easy and time-efficient approach compared to filtration techniques. Magnetic separation is cost-effective and energy-efficient, aligning with green chemistry principles for environmental sustainability. The gold(III) adsorption study using Fe_3O_4/SiO_2/Chitosan was conducted in a batch system. Before adding the adsorbent to the adsorbate, the pH was checked using a pH meter. Subsequently, some adsorbents were added to the gold solution with pH values of 1, 2, 3, 4, 5, and 6, and shaken for 2 h.

Overall, an increase in pH values was observed after the adsorption process. The pH increase in the solution predicts the displacement of H^+ ions from the solution to the adsorbent with amine groups ($-NH_2$). This phenomenon is known as amine group protonation forming $-NH_3^+$ groups. The movement of H+ ions from the solution to the adsorbent surface reduces H+ species in the solution, thereby increasing the pH (decreasing acidity).

The active sites on the adsorbent and adsorbate play a crucial role in the adsorption process, which significantly influences their interactions. Understanding related metal species in the solution system, in this case gold, can be studied through a gold speciation diagram. At low pH, protonated amine species became $-NH_3^+$, while gold(III) complexes dominated as $AuCl_4^-$. Other studies have confirmed that at pH 3-9, chloro-hydroxo complexes begin to form, where the chloride groups are replaced by hydroxide groups with increasing pH, forming $[AuCl_3(OH)]^-$, $[AuCl_2(OH)_2]^-$, $[AuCl(OH)_3]^-$, and at pH above 9, the dominant species is $[Au(OH)_4]^-$[24]. More OH^- groups in

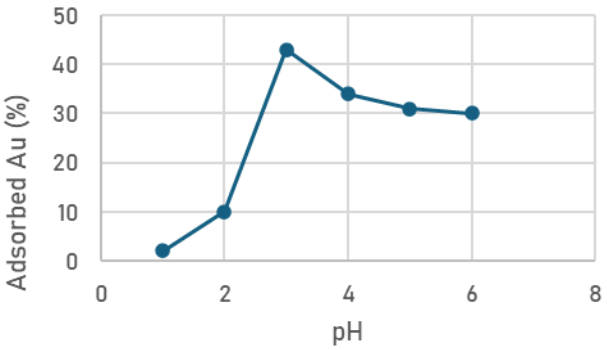

Fig. 5. Effect of pH on adsorbed Au

the solution lead to the formation of more gold hydroxide complexes. Hydroxide complexes have relatively low solubility, forming precipitates that can interfere with the adsorption process.

The effect of pH on the gold(III) adsorption by Fe_3O_4/SiO_2/Chitosan is presented in **Fig. 5**. The amount of gold adsorbed was relatively low at pH 1 and 2, increased until pH 3, and then decreased until pH 6. At pH below 3, the adsorbed gold amount is relatively low, explained by the abundance of chloride ions (Cl^-) even with maximum protonation, causing $-NH_3^+$ groups on the adsorbent to be surrounded by unbound Cl^- not attached to gold. The abundance of chloride ions may lead to competition in the gold(III) adsorption process between Cl^- ions and $AuCl_4^-$ species. The low adsorption values at pH below 3 may also result from magnetite leaching due to excessively acidic conditions, causing ineffective separation of the adsorbent from the adsorbate system as magnetic material detaches from the adsorbent framework. The low adsorption values at pH above 4 may be due to insufficient protonation of amine groups, while gold remains dissolved as negatively charged complexes.

Based on **Fig. 5**, the optimum gold(III) adsorption occurred at pH 3. This can be explained as at pH 3, the amine species are fully protonated (optimum protonated amine amount), while the amount of $AuCl_4^-$ is proportional to protonated amines, with a moderate abundance of chloride ions (Cl^-) in the gold chloride solution system. There are two interaction predictions: between protonated amines and $AuCl_4^-$ and between unprotonated amines and gold(III) **(Fig. 6).** The first interaction is an ionic interaction between protonated amine groups acting as Lewis acids while $AuCl_4^-$ acts as a Lewis base. The second interaction occurs through the chelation of $-NH_2$ groups with gold(III), leading to the replacement of chloride ligands, where two amine groups replace chloride ions [25].

A more logical prediction is the first mechanism involving ionic interactions between the protonated amines and the chloride anions. The optimum adsorption condition at pH 3 suggests that amine groups are in a protonated state, while gold(III) is in the $AuCl_4^-$ species. The adsorption mechanism of gold(III) in $AuCl_4^-$ by the adsorbent through ionic bonding is supported by data showing changes in the pH values

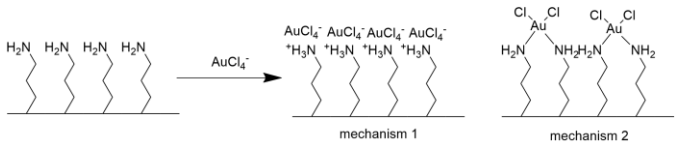

Fig. 6. Prediction of the interaction between the active site amine and gold(III) chloride solution

before and after adsorption, as presented in **Table 2.**, which indicates an increase in the pH values. In the second interaction, the unprotonated amine groups undergo chelation with gold(III), resulting in the release of two Cl^- ligands. The release of Cl^- ions in the solution leads to the formation of HCl, increasing the solution's acidity (decreasing the pH). The data on increased pH values after adsorption do not support chelation interaction by the amine groups, making the second interaction less logical. Ionic interactions are more suitable for the gold(III) adsorption process with the Fe_3O_4/SiO_2/Chitosan adsorbent as conducted.

Table 2. Alterations in the pH of the gold(III) solution were observed before and after the adsorption process.

pH	Before	After
1	1.250	1.250
2	2.260	2.420
3	3.211	3.574
4	4.058	4.569
5	5.063	5.282
6	5.874	6.065

CONCLUSION

The successful incorporation of Fe_3O_4 and Fe_3O_4/SiO_2 into Chitosan resulted in a magnetic nanocomposite, as evidenced by material characterization. The Fe_3O_4/SiO_2/Chitosan formation was achieved through the deposition of Fe_3O_4 with silica modified by Chitosan. The optimal amount of Chitosan to be combined with Fe_3O_4:SiO_2 (0.5:0.73) was determined to be 0.050 g. The successful coating was confirmed through various characterization techniques. The optimal pH for gold(III) adsorption by Fe_3O_4/SiO_2/Chitosan as an adsorbent was at pH 3.

SUPPORTING INFORMATION

There is no supporting information in this paper. The data that support the findings of this study are available on request from the corresponding author (A.R. Pradipta).

ACKNOWLEDGEMENTS

The author would like to thank the Institute for Research and Community Service (PPM) of Polytechnic of AKA Bogor and Universitas Gadjah Mada for permitting the use of the research facilities.

CONFLICT OF INTEREST

The authors have no conflict of interest in this publication.

AUTHOR CONTRIBUTIONS

ARP and RAWP conducted the experiments and interpretation. ARP, RAWP, IYK, and LAH wrote and revised the manuscript. All authors agreed to the final version of this manuscript. All authors agreed to the final version of this manuscript.

REFERENCES

[1] Minnaar, A. 2020. *Water Pollution and Contamination from Gold Mines: Acid Mine Drainage in Gauteng Province, South Africa* in In: Eman, K., Meško, G., Segato, L., Migliorini, M. (eds) Water,

Governance, and Crime Issues. Springer, Cham. pp. 193–219. doi: 10.1007/978-3-030-44798-4_12

[2] Carolin, C.F., Kumar, P.S., Saravanan, A., Joshiba, G.J., & Naushad, M. 2017. Efficient techniques for the removal of toxic heavy metals from aquatic environment: A review. *J. Environ. Chem. Eng.* 5(3). 2782–2799. doi: 10.1016/j.jece.2017.05.029.

[3] Vidu, R., Matei, E., Predescu, A.M., Alhalaili, B., Pantilimon, C., Tarcea, C., & Predescu, C. 2020. Removal of Heavy Metals from Wastewaters: A Challenge from Current Treatment Methods to Nanotechnology Applications. *Toxics*. 8(4). 101. doi: 10.3390/toxics8040101.

[4] Acheampong, M.A., Meulepas, R.J.W., & Lens, P.N.L. 2010. Removal of heavy metals and cyanide from gold mine wastewater. *J. Chem. Technol. & Biotechnol.* 85(5). 590–613. doi: 10.1002/jctb.2358.

[5] Murakami, H., Nishihama, S., & Yoshizuka, K. 2015. Separation and recovery of gold from waste LED using ion exchange method. *Hydrometallurgy*. 157. 194–198. doi: 10.1016/j.hydromet.2015.08.014.

[6] Gupta, A. *et al.* 2021. A Review of Adsorbents for Heavy Metal Decontamination: Growing Approach to Wastewater Treatment. *Materials (Basel).* 14(16). 4702. doi: 10.3390/ma14164702.

[7] Wang, L.K., Wang, M.-H.S., Shammas, N.K., & Hahn, H.H. 2021. *Physicochemical Treatment Consisting of Chemical Coagulation, Precipitation, Sedimentation, and Flotation BT - Integrated Natural Resources Research* in Wang, L.K., Wang, M-H. S., and Hung, Y-T. Eds. Cham: Springer International Publishing, 265–397. doi: 10.1007/978-3-030-61002-9_6.

[8] Sun, Y., Zhou, S., Chiang, P.-C., & Shah, K.J. 2019. Evaluation and optimization of enhanced coagulation process: Water and energy nexus. *Water-Energy Nexus*. 2(1). 25–36. doi: 10.1016/j.wen.2020.01.001.

[9] Stenina, I., Golubenko, D., Nikonenko, V., & Yaroslavtsev, A. 2020. Selectivity of Transport Processes in Ion-Exchange Membranes: Relationship with the Structure and Methods for Its Improvement. *Int. J. Mol. Sci.* 21(15). 5517. doi: 10.3390/ijms21155517.

[10] Karamikamkar, S., Naguib, H.E., & Park, C.B. 2020. Advances in precursor system for silica-based aerogel production toward improved mechanical properties, customized morphology, and multifunctionality: A review. *Adv. Colloid Interface Sci.* 276. 102101. doi: 10.1016/j.cis.2020.102101.

[11] Nowicki, W. 2019. Structural studies of complexation of Cu(II) with aminosilane-modified silica surface in heterogeneous system in a wide range of pH. *Appl. Surf. Sci.* 469. 566–572. doi: 10.1016/j.apsusc.2018.11.066.

[12] Ngouangna, E.N., Manan, M.A., Oseh, J.O., Norddin, M.N.A.M., Agi, A., & Gbadamosi, A.O. 2020. Influence of (3-Aminopropyl) triethoxysilane on silica nanoparticle for enhanced oil recovery. *J. Mol. Liq.* 315. 113740. doi: 10.1016/j.molliq.2020.113740.

[13] Dufil, Y., Gadenne, V., Carrière, P., Nunzi, J.-M., & Patrone, L. 2020. Growth and organization of (3-Trimethoxysilylpropyl) diethylenetriamine within reactive amino-terminated self-assembled monolayer on silica. *Appl. Surf. Sci.* 508. 145210. doi: 10.1016/j.apsusc.2019.145210.

[14] Pradipta, A.R. & Irunsah, A. 2022. Synthesis of Modified TiO_2 Nanocomposite using Fe_3O_4 and Nickel as Photocatalyst in Reduction of Silver Ions. *Indones. J. Chem. Stud.* 1(1). 8–12. doi: 10.55749/ijcs.v1i1.7.

[15] Pradipta, A.R., Mauludi, K., Kartini, I., & Kunarti, E.S. 2020. Synthesis of Fe3O4/TiO2 Nanocomposite as Photocatalyst in Photoreduction Reaction of CO2 Conversion to Methanol, in *Symposium of Materials Science and Chemistry II*, 2020, 840, 454–458. doi: 10.4028/www.scientific.net/KEM.840.454.

[16] Putro, W.S., Lee, V.Y., Sato, K., Choi, J.-C., & Fukaya, N. 2021. From SiO2 to Alkoxysilanes for the Synthesis of Useful Chemicals. *ACS Omega*. 6(51). 35186–35195. doi: 10.1021/acsomega.1c05138.

[17] Ebisike, K., Okoronkwo, A.E., & Alaneme, K.K. 2019. Adsorption of Cd (II) on chitosan–silica hybrid aerogel from aqueous solution. *Environ. Technol. Innov.* 14. 100337. doi: 10.1016/j.eti.2019.100337.

[18] Sánchez Delgado, G.Y., do C Ferreira, F.H., Paschoal, D.F.S., & Dos Santos, H.F. 2022. The role of tridentate ligands on the redox stability of anticancer gold(III) complexes. *J. Inorg. Biochem.* 236. 111970. doi: 10.1016/j.jinorgbio.2022.111970.

[19] Qiao, C., Ma, X., Wang, X., & Liu, L. 2021. Structure and properties of chitosan films: Effect of the type of solvent acid. *LWT*. 135. 109984. doi: 10.1016/j.lwt.2020.109984.

[20] Sugie, C., Navrotsky, A., Lauterbach, S., Kleebe, H.-J., & Mera, G. 2021. Structure and Thermodynamics of Silicon Oxycarbide Polymer-Derived Ceramics with and without Mixed-Bonding. *Materials (Basel).* 14(15). 4075. doi: 10.3390/ma14154075.

[21] Shao, R., Niu, J., Zhu, F., Dou, M., Zhang, Z., & Wang, F. 2019. A facile and versatile strategy towards high-performance Si anodes for Li-ion capacitors: Concomitant conductive network construction and dual-interfacial engineering. *Nano Energy*. 63. 103824. doi: 10.1016/j.nanoen.2019.06.020.

[22] Yao, M.Z., Liu, Y., Qin, C.N., Meng, X.J., Cheng, B.X., Zhao, H., Wang, S.F., & Huang, Z.Q. 2021. Facile fabrication of hydrophobic cellulose-based organic/inorganic nanomaterial modified with POSS by plasma treatment. *Carbohydr. Polym.* 253. 117193. doi: 10.1016/j.carbpol.2020.117193.

[23] Gierszewska, M., Jakubowska, E., & Olewnik-Kruszkowska, E. 2019. Effect of chemical crosslinking on properties of chitosan-montmorillonite composites. *Polym. Test.* 77. 105872. doi: 10.1016/j.polymertesting.2019.04.019.

[24] Karasyova, O., Ivanova, L., Lakshtanov, L., Lövgren, L., & Sjöberg, S. 1998. Complexation of Gold(III)-Chloride at the Surface of Hematite. *Aquat. Geochemistry*. 4. 215–231. doi: 10.1023/A:1009622915376.

[25] Xi, W. & Haes, A.J. 2019. Elucidation of HEPES Affinity to and Structure on Gold Nanostars. *J. Am. Chem. Soc.* 141(9). 4034–4042. doi: 10.1021/jacs.8b13211.